Ocean surface change detection from remote sensing image based on stochastic similarity measure

Detecção de mudança na superfície oceânica a partir de imagem de sensoriamento remoto baseado em medida de similaridade estocástica

Ian Henrique Teles Braga[1] [iD]**, Vinicius Pereira do Sacramento[1]** [iD]**, Lígia Claudia Castro de Oliveira[2]** [iD]**,
Fátima Nelsizeuma Sombra de Medeiros[3]** [iD] **& Francisco Alixandre Ávila Rodrigues[1]** [iD]

[1]Universidade Federal do Cariri, Juazeiro do Norte, CE, Brasil
[2]Universidade Regional do Cariri, Crato, CE, Brasil
[3]Universidade Federal do Ceará, Fortaleza, CE, Brasil

E-mails: ianhenrique.eng@gmail.com (IHTB), vinicius.sacramento@ufca.edu.br (VPS), ligia.castro@urca.br (LCCO), fsombraufc@gmail.com (FNSM), alixandre.avila@ufca.edu.br (FAAR)

ABSTRACT

Change detection based on remote sensing images, has attracted increasing attention from researchers throughout the world. The synthetic aperture radar (SAR) images have become key resources for detecting changes on the land surface. However, due to the presence of speckle noise and its stochastic nature, SAR data require methodologies that consider these peculiarities. This article presents a similarity measure that considers the randomness present in SAR data. To retrieve the random component in the SAR data, we used the stochastic distance. The similarity measure is carefully elaborated as a function of the stochastic distance such that its variation space is the interval [0, 1], facilitating its interpretation. Our proposal shows promising results in two applications: contrast evaluation, ocean surface change detection and binary change map. It is noteworthy that the possible limitations of our proposal are investigated through simulations guided by a Monte Carlo experiment.

Keywords: SAR images; Stochastic distance; Similarity measure; Ocean surface change detection.

RESUMO

A detecção de mudanças com base em imagens de sensoriamento remoto tem atraído cada vez mais atenção de pesquisadores em todo o mundo. As imagens de radar de abertura sintética (SAR) tornaram-se recursos fundamentais para detectar mudanças na superfície terrestre. No entanto, devido à presença do ruído *speckle* e sua natureza estocástica, os dados SAR requerem metodologias que considerem essas peculiaridades. Este artigo apresenta uma medida de similaridade que considera a aleatoriedade presente nos dados SAR. Para recuperar o componente aleatório nos dados SAR, usamos distância estocástica. A medida de similaridade foi cuidadosamente elaborada em função da distância estocástica de forma que seu espaço de variação fosse o intervalo [0, 1], facilitando sua interpretação. Nossa proposta mostra resultados promissores em duas aplicações: avaliação de contraste, detecção de mudanças na superfície oceânica e mapa binário de mudanças. Vale ressaltar que as possíveis limitações de nossa proposta foram investigadas por meio de simulações guiadas por um experimento de Monte Carlo.

Palavras-chave: Imagens SAR; Distância estocástica; Medida de similaridade; Detecção de mudanças na superfície do oceano.

INTRODUCTION

Due to its independence from sunshine conditions, the processing of synthetic aperture radar (SAR) images has furthered important advances in the scientific research of the remote sensing community. Examples include segmentation and identification of oil patches in the sea (Marques et al., 2012; Huang et al., 2005; Ivanov & Ermoshkin, 2004), mapping of the extent of natural disasters such as floods (Long et al., 2014), mapping of underground rivers in arid areas (Skonieczny et al., 2015), mapping of terrestrial surface waters (Xu et al., 2016), mapping of various biophysical properties in forests (Jesus & Kuplich, 2020), changes detection (Yang et al., 2006; Barreto et al., 2016; Jia et al., 2019, 2020; Li et al., 2021), and other fields. The large number of applications of SAR systems is mainly due to the unique characteristics of this type of radar since it provides high-resolution two-dimensional images, independent of daylight, cloud cover and climatic conditions (Moreira et al., 2013). However, the images formed by this system are damaged by multiplicative noise called speckle.

Due to its stochasticity, statistical approaches are usually necessary to address speckle noise. Therefore, the choice of an adequate probability distribution to describe SAR data is of fundamental importance. Here, we opted for the G_I^0 distribution to describe the intensity of SAR data. Frery et al. (1997) present this distribution as a good alternative for this task since it enables the modeling of homogeneous, heterogeneous and extremely heterogeneous regions of SAR data. Contrast analysis is an important task for understanding SAR images. The derivation of contrast measures can be useful to quantify how distinct two regions in an image are. In this context, we can highlight the stochastic distances (Nascimento et al., 2010) as possible measures of contrast.

Based on stochastic distances, Marques et al. (2012) presented a segmentation measure called difficulty of segmentation, hereinafter called DoS. Because its construction considers the concept of stochastic distance, DoS was used in this study as a measure of contrast evaluation. Although quite interesting, this measure has some limitations. For example, when applied to regions with similar DoS, this parameter tends to infinity, and when applied to equivalent regions, DoS cannot be calculated because in this case, there is an undefined mathematical. To circumvent this problem, we present in this article an improved version of the DoS metric. This new measure was successfully applied to two different SAR image processing problems: contrast evaluation and change detection. In particular, our proposal contributes to solving change detection problems in SAR images such as: i) generating a change measure or the change indicator and ii) allowing the use of the change measure threshold to produce a binary change map.

Over the last several decades, various change detection approaches have been developed. The review article (Asoka & Anitha, 2019) gives a brief account of the main techniques of change detection and discusses the need for development of enhanced change detection methods. According to the authors of the article, change detection techniques that present information about areas of change in the form of a binary map showing significant changes are desirable. Our method allows us to obtain binary maps showing changes, thus guaranteeing one of the qualities expected of a change detection method.

Shafique et al. (2022), present deep learning techniques, such as supervised, unsupervised, and semi-supervised for different change detection datasets, such as SAR, multispectral, hyperspectral, VHR, and heterogeneous images, highlighting its challenges. The authors point out that image pre-processing may have a significant beneficial impact on the quality of feature extraction and image analysis outcomes. A feature that we consider important in our proposal is that it does not require pre-processing steps for the SAR images, such as filtering. All information contained at the pixel level is captured through the probability distribution Gi0, and supplied to the method.

The rest of this paper is organized as follows: In Section 2, we presented the proposed methodology and all theoretical background used, followed by the experiments and results in Section 3. Finally, Section 4 summarizes our findings and conclusions.

MATERIAL AND METHODS

Statistical model for SAR data

To describe the Z return of the SAR system, we used the G_I^0 distribution. The function probability density of the G_I^0 distribution is defined as:

$$f_{G_I^0}(z, \alpha, \gamma, L) = \frac{L^L(L-\alpha)z^{L-1}(\gamma + Lz)^{\alpha - L}}{\gamma^\alpha \Gamma(-\alpha)\Gamma(L)} \qquad (1)$$

with the r-th noncentral moment given by:

$$E_{G_I^0}\left[Z^r\right] = \left(\frac{\gamma}{L}\right)^r \frac{\Gamma(-\alpha - r)\Gamma(L + r)}{\Gamma(-\alpha)\Gamma(L)}, \alpha < -r, \qquad (2)$$

where, $z > 0$, $\alpha < 0$ is the roughness parameter, $\gamma > 0$ is the scale parameter, $L > 0$ is the number of looks, and $\Gamma(.)$ is the gamma function. The G_I^0 distribution facilitates the description of homogeneous, heterogeneous, and extremely heterogeneous regions in SAR images intensity (Frery et al., 1997). This characteristic can be considered an advantage because it is not found in other probability distributions used to model SAR data, such as the K and Weibull distributions (Gao et al., 2013).

Parameter estimation.

The log-cumulative method (LCM) has been used with satisfactory results in SAR image processing, especially for small samples, and is a critical method in several applications (Krylov et al., 2013). There are studies in the literature that use the parameters estimated by the log-cumulative method as input to guide classification methods (Singh & Datcu, 2013) and the detection of changes in SAR images (Bujor et al., 2004). The LCM formulation is described below. Let Z be a continuous random variable with probability density function $f_Z(z, \theta)$ defined in R^+. The LCM is based on the Mellin transform of $f_Z(z, \theta)$ (Nicolas, 2002; Gao et al., 2013; Tison et al., 2004; Cheng et al., 2013) given by:

$$\phi_Z(s) = \int_0^\infty u^{s-1} f_Z(u, \theta) du \qquad (3)$$

s is a complex number with a unitary norm (Nicolas, 2002). The log-moment of order v can be obtained by:

$$\widetilde{m_v} = \frac{d^v \phi_z(s)}{ds^v}\big|_{s=1}, v \in N^*$$ (4)

By applying the natural logarithm of $\phi_Z(s)$, we can obtain the log-cumulant of order v as (Nicolas, 2002; Cheng et al. 2013):

$$\widetilde{k_v} = \frac{d^v \psi_z(s)}{ds^v}\big|_{s=1}, v \in N^*$$ (5)

with $\psi_z(s) = \log((\phi_z(s))$. The strategy of the log-cumulative method for estimating the parameters of the G^0_1 distribution is based on the relationship between the log-moments and log-cumulants given by:

$$\widetilde{k_1} = \widetilde{m_1}$$
$$\widetilde{k_v} = \widetilde{m_v} - \sum_{i=1}^{v-1} \binom{v-1}{i-1} \widetilde{k_1} - \widetilde{m_{v-1}}, v \in \{2,3,...\}$$ (6)

In general, $\widetilde{k_v}$ is a function of the vector of parameters, and therefore, the estimation of the parameters is achieved by replacing $\widetilde{m_v}$ with the corresponding sample logmoment, which is given by Nicolas (2002):

$$\widehat{m_v} = \frac{1}{n} \sum_{i=1}^{n} \log z_i^v$$ (7)

where z_i, i $\in$ {1, 2, ..., n}, is a sample of the random variable Z.

For the probability distribution G^0_1, the estimation of the parameters α, γ and L consists of solving the system of nonlinear equations of the Equation 8 (Cui & Datcu, 2011):

$$\tilde{k}_1 = \log\left(\frac{\gamma}{L}\right) + \psi^0(L) - \Psi^0(-\alpha)$$
$$\tilde{k}_2 = \Psi^1(L) - \Psi^1(-\alpha)$$ (8)
$$\tilde{k}_3 = \Psi^2(L) - \Psi^2(-\alpha)$$

The functions $\Psi^0(.)$, $\Psi^1(.)$ and $\Psi^2(.)$ cannot be inverted, so the solution of the system of equations in (8) cannot be obtained explicitly, and therefore, numerical procedures are necessary.

Stochastic distance

Stochastic distances are useful for investigating whether two random samples can be considered realizations of the same probability distribution. A list of stochastic distances is presented in (Nascimento et al., 2010), among which is the arithmetic geometric distance (Taneja, 1995) adopted here. The mathematical formalization of this stochastic distance is presented below. Let Z_1 and Z_2 be continuous random variables defined in the same probability space, with probability density functions $f_{Z1}(z, \theta_1)$ and $f_{Z2}(z, \theta_2)$, respectively, where θ_1 and θ_2 are vectors of parameters. Assuming that both densities share a common basis, the arithmetic-geometric stochastic distance between $f_{Z1}(z, \theta_1)$ and $f_{Z2}(z, \theta_2)$ is given by (Nascimento et al., 2010):

$$d_{ag}(Z_1, Z_2) = \frac{1}{2} \int (f_{z1} + f_{z2}) \log\left(\frac{f_{z1} + f_{z2}}{2\sqrt{f_{z1}f_{z2}}}\right)$$ (9)

Next, we present the definition of the DoS measure. This measure was used in some applications in this study and inspired us to develop a new similarity measure.

Difficulty of segmentation

Marques et al. (2012) proposed a measure whose initial objective is to evaluate the segmentation of SAR images. Using the concept of the stochastic distance, the measure quantifies the contrast between the background and foreground in SAR images. The authors noted this measure as DoS, expressed as:

$$DoS(Z_1, Z_2) = \frac{1}{d_{ag}(Z_1, Z_2)}$$ (10)

where $d_{ag}(Z_1, Z_2) \geq 0$ is the arithmetic-geometric stochastic distance between two random variables Z_1 and Z_2. A list of stochastic distances is presented in (Nascimento et al., 2010).

Proposed method

DoS, represented in Equation 10, is a way to quantify contrast in SAR images. Based on this concept, it is reasonable to consider DoS to be a measure of similarity between regions, with the possibility of different applications. However, DoS has some limitations that may hinder interpretations. As the stochastic distance between two regions approaches zero, DoS tends to infinity. On the Other hand, when the stochastic distance between two regions is zero, it is not possible to obtain DoS because in this case, there is an undefined mathematical operation. In summary, DoS presents difficulties in the interpretation between very similar or low contrast regions. To circumvent the limitations of DoS, we propose the following correction:

$$DoS_{mod}(Z_1, Z_2) = \frac{1}{e^{d_{ag}(Z_1, Z_2)}}$$ (11)

with e being the Euler-Mascheroni constant (Arfken & Weber 2005). With this modified version of DoS, the limitations are overcome. The variation spaces of DoS_{mod} and DoS can be mapped from the values that d_{ag} can assume. Using the concept of limit, we can verify that when d_{ag} tends to $+\infty$, both DoS_{mod} and DoS tend to 0, see Equations 12 and 13:

$$lim_{d_{ag} \to +\infty} \frac{1}{e^{d_{ag}}} = 0$$ (12)

$$lim_{d_{ag} \to +\infty} \frac{1}{d_{ag}} = 0$$ (13)

On the other hand, when d_{ag} approaches zero from the right, DoS_{mod} tends to 1, and DoS tends to $+\infty$. Equations 14 and 15 show these behaviors.

$$lim_{d_{ag} \to 0} \frac{1}{e^{d_{ag}}} = 1$$ (14)

$$lim_{d_{ag} \to 0} \frac{1}{d_{ag}} = +\infty$$ (15)

However, when SD = 0, DoS is mathematically undefined, while DoS_{mod} = 1. Therefore, $DoS_{mod} \in [0, 1]$ and $DoS \in [0,+\infty)$. DoS also exhibits an abrupt decay in its value (Figure 1(a)). This behavior is not observed in DoS_{mod} (Figura 1(b)). To demonstrate the advantages of DoS_{mod} over DoS, we performed experiments with simulated and real data. Descriptions of the experiments are given in the following section.

Experiments to validate DoS_{mod}

Experiments with simulated SAR data

To evaluate the performance of the proposed method, a Monte Carlo experiment was performed. This experiment was performed with the software R version 4.1.1 in a computer with a 2.20 GHz CPU with 4 GB of RAM, and the processing time was 106.36 seconds. Using the simulation procedure, random samples of the GI0 distribution were generated by combining the parametric spaces $\alpha \in \{-1.5, -3, -5, -8, -12\}$, $L \in \{1, 3, 5, 8\}$ and without loss of generality, the scale parameters were chosen in such a way that $E_{GI0}[Z_I] = 1$. Note that each combination represents a scenario; that is, twenty scenarios were evaluated. The steps of the Monte Carlo experiment are described below:

- Step 1: Simulate two random vectors (vi,1, vi,2) of size n from the GI0 Distribution with parameters according to the scenario Ci, i $\in$ {1, 2, 3, ..., 20}.
- Step 2: Calculate dAG(vi,1, vi,2) and DoSmod(vi,1, vi,2).

- Step 3: Repeat steps 1 and 2, K times.

In this study, n = 100 and K = 1000 were used. The objective of the Monte Carlo experiment was to verify the influence of the intrinsic variability of the probability distribution on the results of DoS_{mod}.

Experiments with real SAR data

First, we investigated the performance of our proposed method in terms of the evaluation of contrasts. For this purpose, clippings from different regions of a real SAR image with different intensity were obtained, DoS_{mod} and DoS were calculated between each pair of clippings, and the results were evaluated. Another important application of our proposal was to detect changes. The flowchart of Figure 2 shows the two steps of the change detection algorithm.

The input data of the algorithm are two SAR images from the same region taken at different times, i.e., bitemporal SAR images. Inspired by the idea of Mejail et al. (2003), the algorithm calculates DoS_{mod} between corresponding pixels of the bitemporal images. The result of the algorithm is an image that represents the similarities between the images. In this study, this image is denoted by a matrix indicator changes (MIC). An important aspect of the MIC is that it presents small changes (DoS_{mod} close to 1) to significant changes (DoS_{mod} close to zero). From the MIC, we can generate maps showing the most significant changes using a thresholding process.
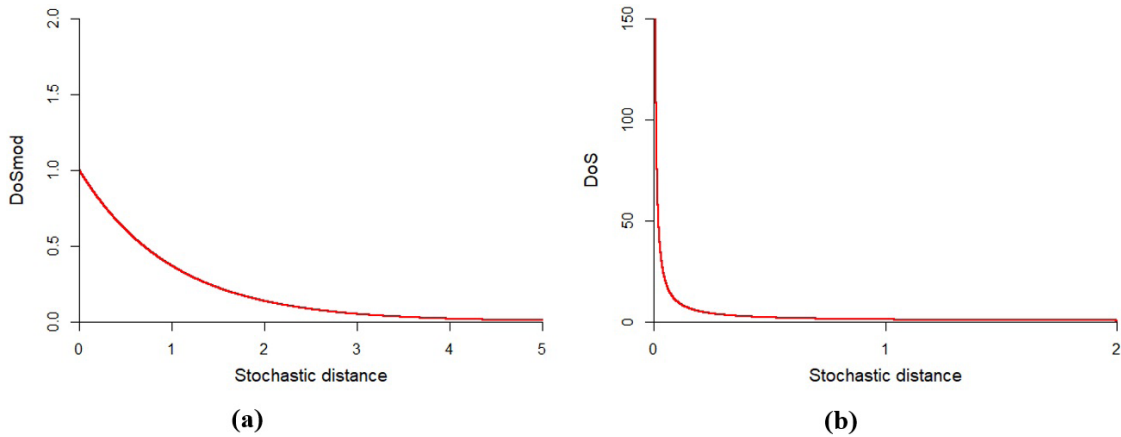

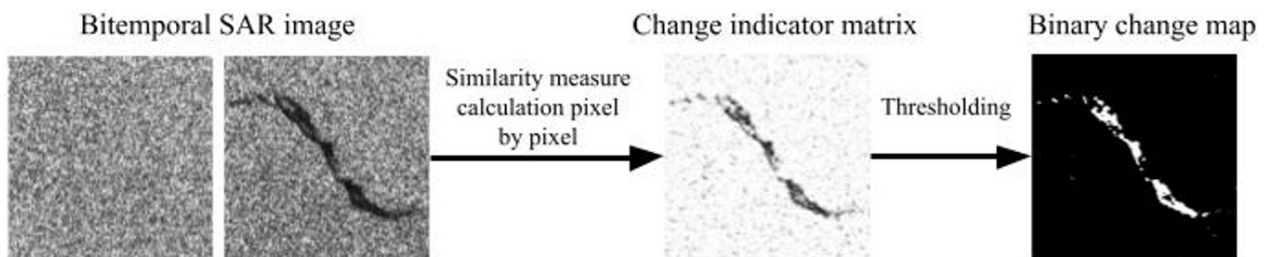**Figure 1.** Comparison between DoS and DoS_{mod}.

Figure 2. Flowchart for the change detection methodology.
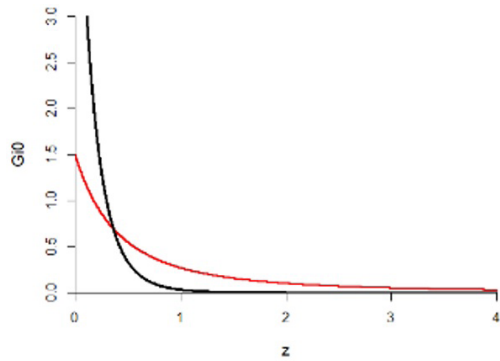
RESULTS

Results with simulated SAR data

The results of the Monte Carlo experiment can highlight some situations that are less or more favorable in terms of the use of DoS_{mod}. Table 1 shows the results of the Monte Carlo experiment. We can observe that, in general, as the number of looks (L) increases, the stochastic similarity (DoS_{mod}) increases, and the standard deviation decreases, thus revealing the importance of the L parameter in the sensitivity of our proposal (DoS_{mod}). This behavior is expected because the number of looks can be considered a control parameter of the speckle noise; that is, the greater the number of looks, the less influence the noise has. Therefore, the experiments show that where there is a greater presence of the speckle, applying DoS_{mod} is more challenging.

Regarding the influence of the roughness parameter (α) in our proposal, the Monte Carlo experiment reveals that this parameter is very sensitive when L = 1, the most challenging case. From the first column of results in Table 1, we can see that DoS_{mod} results increase significantly and that the standard deviations decrease from extremely heterogeneous regions ($\alpha = -1.5$) to homogeneous regions ($\alpha = -12$). These behaviors identified from the Monte Carlo experiment are associated with a greater or lesser presence of speckle noise. One of the implications of speckle noise is its ability to reduce contrast in SAR images as the contrast value decreases. In terms of probability distribution, noise affects the form of the distribution. In the case of the G_I^0 distribution, when the noise is milder, it leads to a greater kurtosis (widening of the distribution shape); otherwise, a lower kurtosis occurs. Figure 3 allows us to visualize the combinations of parameters of the G_I^0 distribution that results in lower or higher kurtosis.

**Table 1.** Mean values and standard deviations for DoS_{mod} from the Monte Carlo experiment.

| α	L=1	L=3	L=5	L=8
-1.5	(0.7292 ± 0.2645)	(0.9349 ± 0.0857)	(0.9614 ± 0.0466)	(0.9719 ± 0.0335)
-3.0	(0.8643 ± 0.1706)	(0.9664 ± 0.0414)	(0.9865 ± 0.0175)	(0.9911 ± 0.0091)
-5.0	(0.8920 ± 0.1474)	(0.9804 ± 0.0252)	(0.9924 ± 0.0082)	(0.9930 ± 0.0063)
-8.0	(0.9099 ± 0.1218)	(0.9873 ± 0.0165)	(0.9931 ± 0.0063)	(0.9925 ± 0.0069)
-12.0	(0.9165 ± 0.1205)	(0.9888 ± 0.0134)	(0.9928 ± 0.0068)	(0.9935 ± 0.0056)

a) Black line: ($\alpha = -1.5$, $\gamma = 1$, L = 1).
Red line: ($\alpha = -12$, $\gamma = 1$, L = 1).
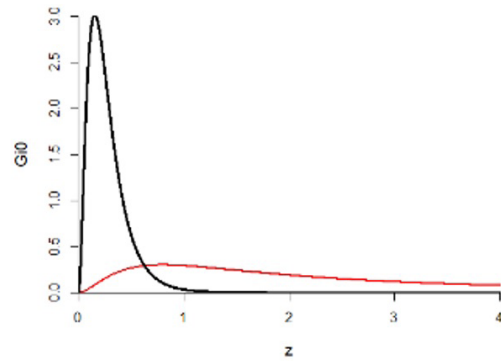
(b) Black line: ($\alpha = -1.5$, $\gamma = 3$, L = 3).
Red line: ($\alpha = -12$, $\gamma = 3$, L = 3).
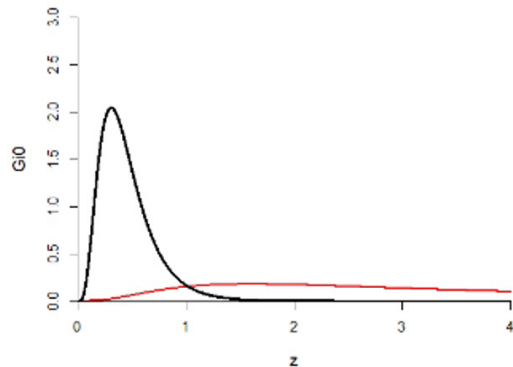
c) Black line: ($\alpha = -1.5$, $\gamma = 5$, L = 5).
Red line: ($\alpha = -12$, $\gamma = 5$, L = 5).
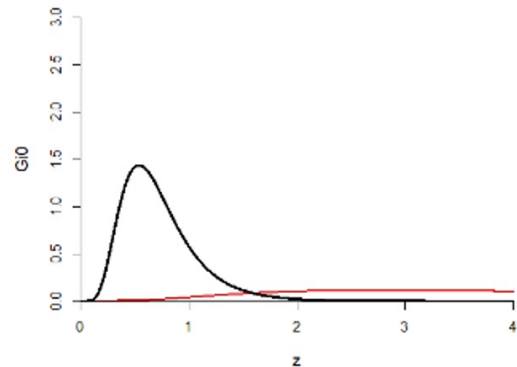
d) Black line: ($\alpha = -1.5$, $\gamma = 8$, L = 8).
Red line: ($\alpha = -12$, $\gamma = 8$, L = 8.

Figure 3. View of the Monte Carlo experiment from the G0I distribution.

Results with real SAR data

Contrast evaluation

To verify the performance of DoS_{mod} and DoS in the evaluation of contrast in real SAR images, clippings were taken from different regions of the San Francisco Bay image (USA), as shown in Figure 4. This image was obtained by the Airborne SAR (AIRSAR) sensor, with the HH polarization channel and 3 looks.

The image shows 3 different types of regions: i) homogeneous (clippings 1 and 2, corresponding to water); ii) heterogeneous (clippings 3 and 4, vegetation); and iii) extremely heterogeneous (clippings 5 and 6, urban areas). For each pair of clippings, DoS and DoS_{mod} measures were calculated, and the values are shown in Tables 2 and 3, respectively. The asterisks in Table 2 are reflections of the mathematical definition of DoS, something that does not occur with DoS_{mod} (see Table 3). In general, we can observe in Tables 2 and 3 that the results for DoS_{mod} are more intuitive to interpret, as $DoS \in [0,\infty)$ and $DoS_{mod} \in [0, 1]$. This experiment was
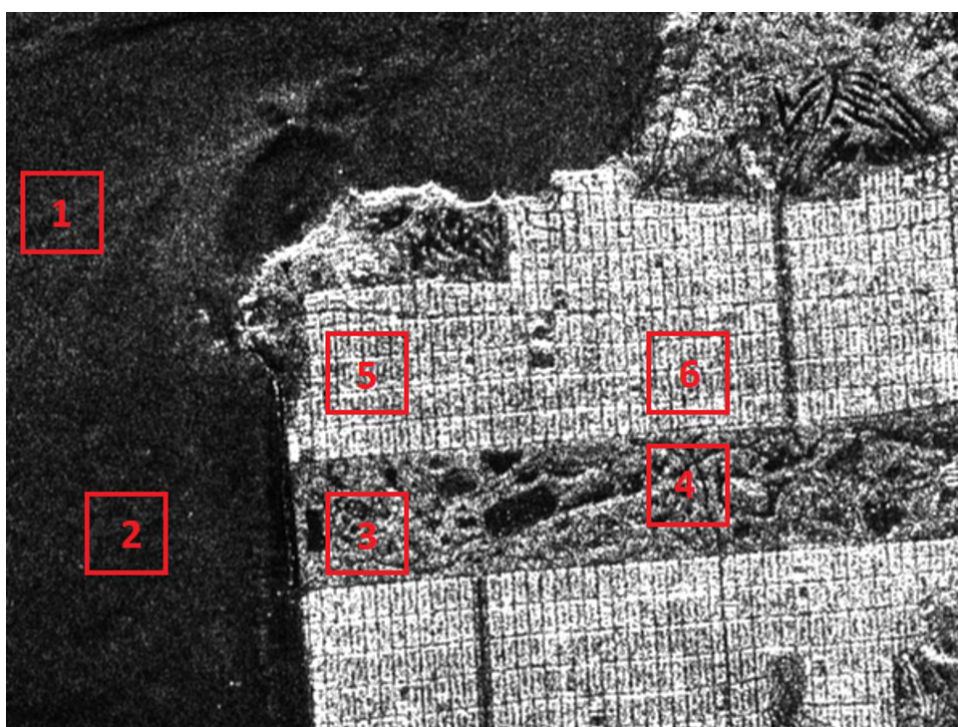

Figure 4. Real SAR image – San Francisco Bay (USA), with 50x50 pixel clippings.

Table 2. Values for segmentation difficulty (DoS).

Clippings	1	2	3	4	5	6
1	*					
2	4.0850	*				
3	0.8130	0.4246	*			
4	0.9727	0.4633	0.0081	*		
5	0.3581	0.2365	5.0813	3.3761	*	
6	0.3367	0.2299	4.1408	2.8035	277.7778	*

* means mathematically undefined.

Table 3. Values for the measurement of the stochastic similarity (DoSmod).

Clippings	1	2	3	4	5	6
1	1.0000					
2	0.7828	1.0000				
3	0.2921	0.0949	1.0000			
4	0.3577	0.1155	0.9920	1.0000		
5	0.0612	0.0145	0.8214	0.7437	1.0000	
6	0.0513	0.0129	0.7854	0.6999	0.9963	1.0000

important for verifying how the measures behave when applied to different intensity conditions in real SAR images.

Application to change detection in ocean surface

Inspired by the idea of Mejail et al. (2003), we calculated the parameters for each pixel of the multitemporal images using a 5x5 pixel window from the log-cumulant method. From the pixel-by-pixel calculation of the arithmetic-geometric stochastic distance between the images, it was possible to obtain the DoS matrix shown in Figure 5(c). In parallel, it was possible to obtain the DoSmod matrix shown in Figure 5(d), which displays pixels with DoS_{mod} values. These two matrices are considered here to be MICs. After the results were obtained, the computational time consumed to obtain the change indicator matrix was measured. This process requires the time taken for each of the steps present in the flowchart of Figure 2.

This experiment was performed with R version 4.1.1 in a computer with a 2.20 GHz CPU with 4 GB of RAM, and the processing time was 135.5 seconds. Figures 5(a) and 5(b) show SAR images of the same region obtained at different times by the RADARSAT sensor, with 1 look and the HH polarization channel. We can verify the appearance of a dark spot and the presence of a shiny object, but they are not perceptible at the pixel level (due to the speckle noise).

In another analysis, we calculated the MIC for another multitemporal scenario with real SAR images of the Brazilian Northeast coast obtained by the RADARSAT sensor, with 3 looks and HH polarization, shown Figures 6(a) and 6(b). For both cases, we can see that the change indicator matrices are able to capture the changes in the scenes. The MIC generated from DoS_{mod} allows interpretation of the measurements. Using MIC, we can build a binary change map. For this, we just use a simple thresholding procedure, like, replace the pixel at position (x, y) by zero if the DoS_{mod} at the position (x, y) is less than p ∈ (0, 1) and 1 otherwise. The Figure 7, shows the binary change map (for p = 0.6) of the DoS_{mod} matrix of the Figure 6(d). Here, it is worth mentioning the flexibility of our proposal in being able to generate binary change map from the choice of p.
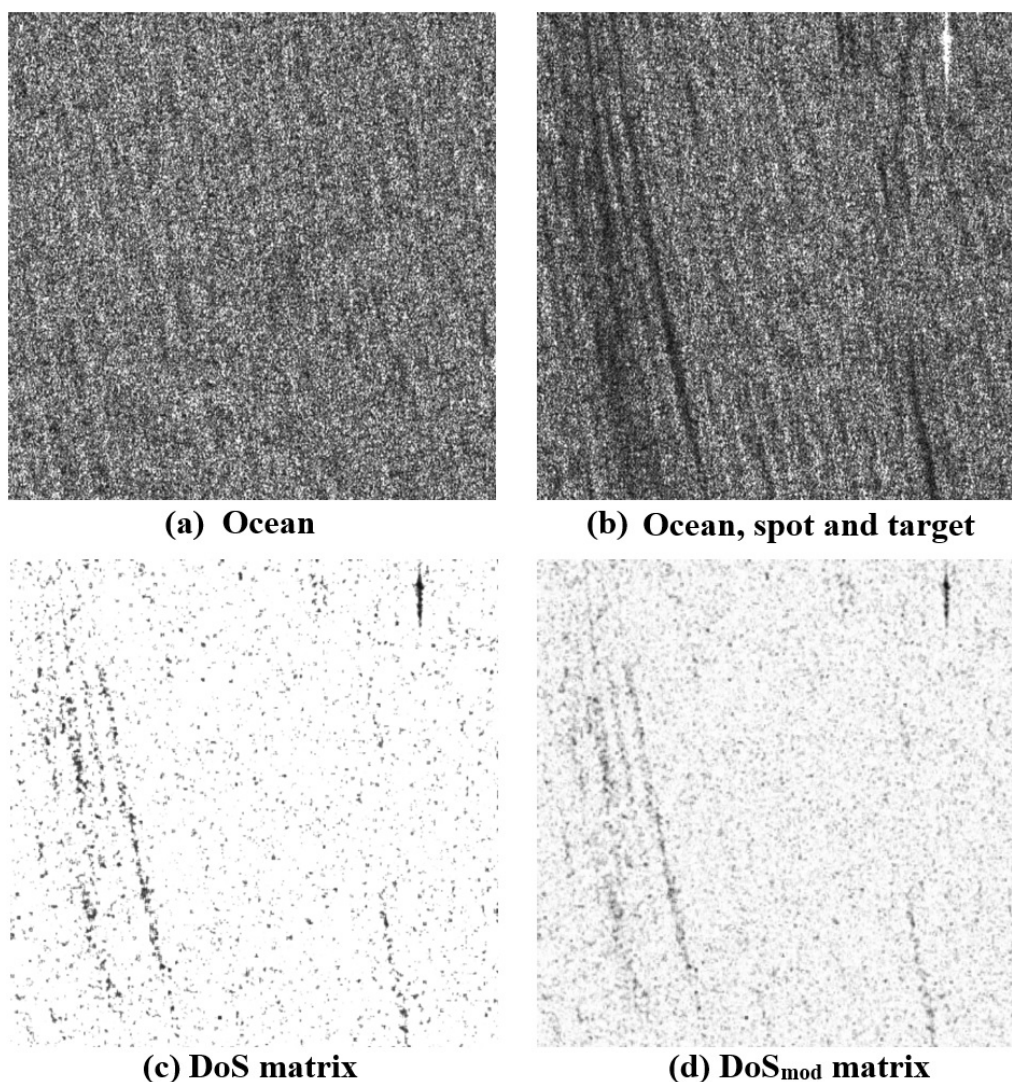

(a) Ocean

(b) Ocean, spot and target

(c) DoS matrix

(d) DoSmod matrix

Figure 5. Real multitemporal SAR image - spot and target at sea.

(a) Sea

(b) Sea and Oil

(c) DoS matrix
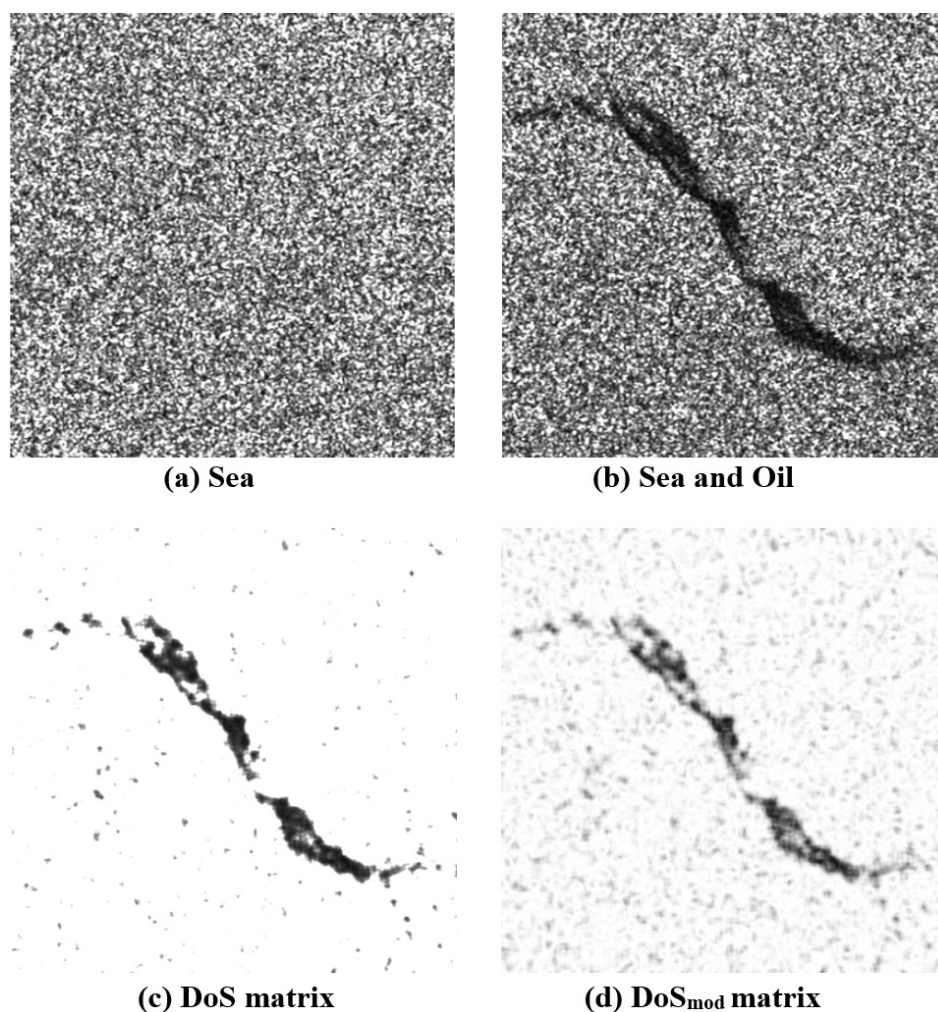

(d) DoS$_{mod}$ matrix

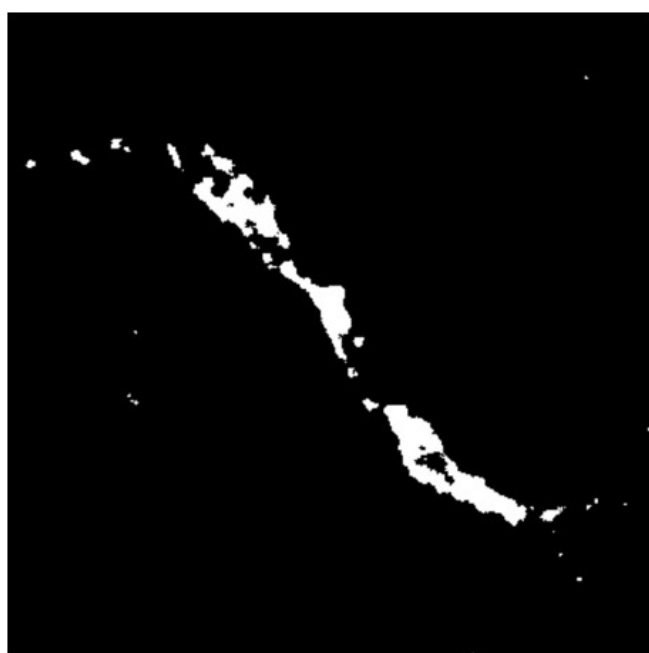**Figure 6.** Real multitemporal SAR image - Oil spot in the sea.

Figure 7. Binary change map of the DoS$_{mod}$ matrix of the Figure 6(d).

CONCLUSION

In the present study, we present a similarity measure (DoS$_{mod}$) obtained with easy integration that may be useful in SAR image processing problems. The experiments with synthetic SAR data revealed that DoS$_{mod}$ is sensitive to small random fluctuations, especially for single look SAR images that have extremely heterogeneous regions. Our proposal was also applied in two experiments with real SAR images. Applying DoS$_{mod}$ to evaluate contrast, we observed that the results could be intuitively interpreted, as DoS$_{mod} \in [0, 1]$. Finally, we used DoS$_{mod}$ to evaluate the detection of changes in ocean surface. The construction of the change indicator matrix was proposed, which was able to capture the most significant changes in the scenarios analyzed. In this sense, our proposed similarity measure can be used in applications with SAR images; however, further studies on the properties of DoS$_{mod}$ can be undertaken to corroborate the developments of this study.

REFERENCES

Arfken, G. B., & Weber, H. J. (2005). *Mathematical methods for physicists*. San Diego, USA: Dover Publications.

Asoka, A., & Anitha, J. (2019). Change detection techniques for remote sensing applications: a survey. *Earth Science Informatics*, *12*, 143-160.

Barreto, T., Rosa, R., Wimmer, C., Moreira, J., Bins, L., Cappabianco, F., & Almeida, J. (2016). Classification of detected changes from multitemporal high-res xband SAR images: intensity and texture descriptors from superpixels. *IEEE Journal of Selected Topics in Applied Earth Observations and Remote Sensing*, *9*(12), 5436-5448.

Bujor, F., Trouve, E., Valet, L., Nicolas, J., & Rudan, J. (2004). Application of logcumulants to the detection of spatiotemporal discontinuities in multitemporal SAR images. *IEEE Transactions on Geoscience and Remote Sensing*, *42*(10), 2073-2084.

Cheng, J., Gao, G., Ding, W., Ku, X., & Sun, J. (2013). An improved scheme for parameter estimation of g distribution model in high-resolution sar images. *Progress in Electromagnetics Research*, *134*, 23-46.

Cui, S., & Datcu, M. (2011). Coarse to fine patches-based multitemporal analysis of very high resolution satellite images. In *6th International Workshop on the Analysis of Multi-Temporal Remote Sensing Images (Multi-Temp)* (pp. 85-88). Trento, Italy: IEEE.

Frery, A. C., Muller, H., Freitas, C. C., & Sant'Anna, S. J. S. (1997). A model for extremely heterogeneous clutter. *IEEE Transactions on Geoscience and Remote Sensing*, *35*(3), 648-659.

Gao, G., Qin, X., & Zhou, S. (2013). Modeling sar images based on a generalized gamma distribution for texture component. *Progress in Electromagnetics Research*, *137*, 669-685.

Huang, B., Li, H., & Huang, X. (2005). A level set method for oil slick segmentation in SAR images. *International Journal of Remote Sensing*, *26*(6), 1145-1156.

Ivanov, A. Y., & Ermoshkin, I. S. (2004). Mapping oil spills in the caspian sea using ers-1/ers-2 sar image quick-looks and gis. *Gayana (Concepción)*, *68*(2), 297-304.

Jesus, J. B. d., & Kuplich, T. M. (2020). Applications of sar data to estimate forest biophysical variables in brazil. *Cerne*, *26*(1), 88-97.

Jia, L., Wang, J., Ai, J., & Jiang, Y. (2020). A hierarchical spatial-temporal graph-kernel for high-resolution sar image change detection. *International Journal of Remote Sensing*, *41*(10), 3866-3885.

Jia, M., Zhao, Z., Huo, L., Chen, H., & Qiu, Y. (2019). Incorporating global-local a priori knowledge into expectation-maximization for sar image change detection. *International Journal of Remote Sensing*, *40*(2), 734-758.

Krylov, V., Moser, G., Serpico, S. B., & Zerubia, J. (2013). On the method of logarithmic cumulants for parametric probability density function estimation. *IEEE Transactions on Image Processing*, *22*(10), 3791-3806.

Li, X., Du, Z., Huang, Y., & Tan, Z. (2021). A deep translation (GAN) based change detection network for optical and SAR remote sensing images. *ISPRS Journal of Photogrammetry and Remote Sensing*, *179*, 14-34.

Long, S., Fatoyinbo, T. E., & Policelli, F. (2014). Flood extent mapping for Namibia using change detection and thresholding with SAR. *Environmental Research Letters*, *9*(3), 1-9.

Marques, R. C. P., Medeiros, F. N., & Nobre, J. S. (2012). SAR image segmentation based on level set approach and GA0 model. *IEEE Transactions on Pattern Analysis and Machine Intelligence*, *34*(10), 2046-2057.

Mejail, M. E., Jacobo-Berlles, J. C., & Frery, A. C. (2003). Classification of SAR images using a general and tractable multiplicative model. *International Journal of Remote Sensing*, *24*(18), 3565-3582.

Moreira, A., Prats-Iraola, P., Younis, M., Krieger, G., Hajnsek, I., and Papathanassiou, K. P. (2013). A tutorial on synthetic aperture radar. *IEEE Geoscience and Remote Sensing Magazine*, *1*(1):6-43.

Nascimento, A. D. C., Cintra, R. J., & Frery, A. C. (2010). Hypothesis testing in speckle data with stochastic distances. *IEEE Transactions on Geoscience and Remote Sensing*, *48*(1), 373-385.

Nicolas, J. (2002). Introduction aux statistiques de deuxi'eme esp'ece: application des logsmoments et des logs-cumulants `a l'analyse des lois d'images radar. *Traitement du Signal*, *19*(3), 139-167.

Shafique, A., Cao, G., Khan, Z., Asad, M., & Aslam, M. (2022). Deep learning-based change detection in remote sensing images: a review. *Remote Sensing*, *14*(4), 871.

Singh, J., & Datcu, M. (2013). Sar image categorization with log cumulants of the fractional fourier transform coefficients. *IEEE Transactions on Geoscience and Remote Sensing*, *51*(12), 5273-5282.

Skonieczny, C., Paillou, P., Bayon, A., Biscara, L., Crosta, X., Eynaud, F., Malaiz'e, B., Revel, M., Aleman, N., Barusseau, J. P., Vernet, R., Lopez, S., & Grousset, F. (2015). Affrican humid periods triggered the reactivation of a large river system in western sahara. *Nature Communications*, *6*, 1-6.

Taneja, I. J. (1995). New developments in generalized information measures. *Advances in Imaging and Electron Physics*, *91*, 37-135.

Tison, C., Nicolas, J.-M., Tupin, F., & Maitre, H. (2004). A new statistical model for markovian classification of urban areas in high-resolution sar images. *IEEE Transactions on Geoscience and Remote Sensing*, *42*(10), 2046-2057.

Xu, C., Sui, H., & Xu, F. (2016). Land surface water mapping using multi-scale level sets and a visual saliency model from SAR images. *International Journal of Geo-Information*, *58*, 1-19.

Yang, J., Xiong, T., & Peng, Y.-N. (2006). Polarimetric sar image classification by using generalized optimization of polarimetric

contrast enhancement. *International Journal of Remote Sensing*, *27*(16), 3413-3424.

Authors contributions

Ian Henrique Teles Braga: Data processing, manuscript writing.

Vinicius Pereira do Sacramento: Methodology, manuscript review.

Lígia Claudia Castro de Oliveira: Experimental planning, Methodology.

Fátima Nelsizeuma Sombra de Medeiros: Experimental planning, Methodology.

Francisco Alixandre Ávila Rodrigues: Experimental planning, manuscript review and writing, Methodology, Project administration.

Editor-in-Chief: Adilson Pinheiro

Associated Editor: Fernando Mainardi Fan